Axially symmetric on-axis flat-top beam

Qing Cao* and Sien Chi

Institute of Electro-Optical Engineering, National Chiao Tung University, 1001 Ta Hsueh Road, Hsinchu, Taiwan 300, China

Received May 28, 1999; revised manuscript received October 22, 1999; accepted October 22, 1999

A synthesis method for arbitrary on-axis intensity distributions from axially symmetric fields is developed in the paraxial approximation. As an important consequence, a new pseudo-nondiffracting beam, the axially symmetric on-axis flat-top beam (AFTB), is given by an integral transform form. This AFTB is completely determined by three simple parameters: the central spatial frequency S_c, the on-axis flat-top length L, and the on-axis central position z_c. When $LS_c \gg 1$, this AFTB can give a nearly flat-top intensity distribution on the propagation axis. In particular, this AFTB approaches the nondiffracting zero-order Bessel J_0 beam when $L \to \infty$. It is revealed that the superposition of multiple AFTB fields can give multiple on-axis flat-top intensity regions when some appropriate conditions are satisfied. © 2000 Optical Society of America [S0740-3232(00)01202-3]

OCIS codes: 050.1940, 350.5500, 220.1140.

1. INTRODUCTION

Nondiffracting beams, such as the zero-order Bessel J_0 beam,[1,2] have attracted much attention, because their intensity distributions do not change in those transverse planes perpendicular to the propagation direction. These novel nondiffracting beams are of practical interest, for example, in precision alignment, laser machining, and laser surgery. However, ideal nondiffracting beams are not realizable in physics because they have infinite energy. Recently many authors have investigated the so-called pseudo-nondiffracting beams.[3–23] A pseudo-nondiffracting beam is characterized by an almost constant axial intensity distribution over a finite axial region and a beamlike shape in the transverse dimensions. Recently many kinds of pseudo-nondiffracting beams have been presented by the use of various methods such as the stationary phase method,[7,14,16,19] the iterative method,[8–11,13,17] and the two-element method.[20–22]

Besides those pseudo-nondiffracting beams whose on-axis intensity distributions are almost invariable in a specific region, those beams whose on-axis intensity distributions have other specific profiles, such as the profile of multiple flat-top intensity regions on the propagation axis, are of practical interest. For example, those axially symmetric beams with multiple on-axis flat-top intensity regions can be used in the laser head of multifocal optical disk drives. In the past few years, several authors have investigated the synthesis problem of arbitrary on-axis intensity distributions in free space by employing various iterative methods.[24–27]

In this paper we shall employ the spatial-frequency method to construct arbitrary on-axis intensity distributions from axially symmetric fields in the paraxial approximation. Based on this construction method, we shall present a new pseudo-nondiffracting beam, the axially symmetric on-axis flat-top beam (AFTB), which can be regarded as a modified version of the paraxial Bessel J_0 beam and investigate its on-axis intensity behavior. In addition, we shall investigate the synthesis problem of multiple on-axis flat-top intensity distributions from the linear superposition of multiple AFTB fields.

2. SYNTHESIS OF ARBITRARY ON-AXIS INTENSITY DISTRIBUTIONS FROM AXIALLY SYMMETRIC FIELDS

In the paraxial approximation, the slowly varying envelope $\phi(x, y, z)$ of an arbitrary monochromatic light beam $E(x, y, z, t) = \exp[i(kz - \omega t)]\phi(x, y, z)$ obeys the following paraxial wave equation[28]:

$$i2k\frac{\partial \phi}{\partial z} + \frac{\partial^2 \phi}{\partial x^2} + \frac{\partial^2 \phi}{\partial y^2} = 0, \tag{1}$$

where k is the wave number and ω is the angular frequency. It is well known that,[28] to a general axially symmetric beam $\phi(r, z)$, the solution of Eq. (1) is given by

$$\psi(f, z) = \psi(f, 0)\exp(-i\pi\lambda f^2 z) \tag{2}$$

in the spatial-frequency domain, where f is the radial spatial frequency, λ is the wavelength, and $\psi(f, z)$ is the Fourier–Bessel transform of the complex optical field distribution $\phi(r, z)$ at the $z = z$ plane, namely,

$$\phi(r, z) = 2\pi\int_0^\infty \psi(f, z)J_0(2\pi r f)f\,\mathrm{d}f, \tag{3}$$

where $J_0(u)$ is the zero-order Bessel function of the first kind.

Substituting Eq. (2) into Eq. (3), one can obtain

$$\phi(r, z) = \int_0^\infty k\psi(\sqrt{2S/\lambda}, 0)\exp(-i2\pi Sz) \times J_0(2\pi r\sqrt{2S/\lambda})\mathrm{d}S, \tag{4}$$

where $S = \lambda f^2/2$. In particular, the on-axis field distribution $\phi(0, z)$ is given by

$$\phi(0,z) = \int_0^\infty k\psi(\sqrt{2S/\lambda},\ 0)\exp(-i2\pi Sz)\mathrm{d}S, \qquad (5)$$

where the property $J_0(0) = 1$ has been used.

From Eq. (5) one can find that the on-axis field distribution $\phi(0,z)$ is the half-space Fourier transform of the function $k\psi(\sqrt{2S/\lambda},\ 0)$ at the original $z = 0$ plane. This property implies that the inverse Fourier transform of the on-axis field distribution $\phi(0,z)$ of an arbitrary axially symmetric field $\phi(r,\ z)$ has no negative spatial-frequency component at all.

It is well known that, in the spatial-frequency domain, the longitudinal spatial frequency f_z is given by $f_z = \lambda^{-1}\sqrt{1-\lambda^2 f^2}$ for an axially symmetric field. In particular, in the paraxial approximation, $\sqrt{1-\lambda^2 f^2} \approx 1 - \lambda^2 f^2/2$, and f_z reduces to $f_z = \lambda^{-1} - S$. From this expression, one can know that the quantity S is directly related to the longitudinal spatial frequency f_z. In the following, we shall also for simplicity call the quantity S the (longitudinal) spatial frequency, because, for a monochromatic optical field, the quantity λ^{-1} is actually a constant. From the relation $S = \lambda f^2/2$, one knows that the longitudinal spatial frequency S is always positive. However, in the remainder of this paper, we shall for convenience extend the longitudinal spatial frequency S to the negative region (i.e., $S < 0$) in form. Unlike the positive longitudinal spatial frequency (i.e., $S \geqslant 0$), the negative longitudinal spatial frequency (i.e., $S < 0$) has no real physical meaning. We shall deal with it only as a variable in some related integral transforms.

Let us now employ the spatial-frequency method to construct an arbitrary on-axis desired intensity distribution $I_g(0,z)$ from an axially symmetric field. Our method is as follows.

First, we obtain the inverse Fourier transform $\varphi(S)$ of the function $\sqrt{I_g(0,z)}$, namely,

$$\varphi(S) = \int_{-\infty}^\infty \sqrt{I_g(0,z)}\exp(i2\pi Sz)\mathrm{d}z. \qquad (6)$$

Usually the function $\varphi(S)$ is complex and has negative spatial-frequency components. However, for the practical case, the function $\varphi(S)$ should have a limited distribution, provided that the integral $\int_{-\infty}^{\infty} I_g(0,z)\mathrm{d}z$ is finite. Fortunately, for practical synthesis problems, the integral $\int_{-\infty}^{\infty} I_g(0,z)\mathrm{d}z$ is always finite. One can deduce that, as an important consequence of the property that the function $\varphi(S)$ has a limited distribution, the integral

$$\int_{-\infty}^{-S_l} \varphi(S)\exp(-i2\pi Sz)\mathrm{d}S$$

decreases (may not monotonously decrease) with the increase of the integral limit S_l in the total behavior. In particular, this integral approaches 0 when $S_l \to \infty$.

Second, we replace the variable S of the function $\varphi(S)$ by the variable $S - S_c$ and construct a new function $\varphi(S - S_c)$, where S_c is a positive parameter. The effect of this step is to reduce the negative spatial-frequency components, because the negative spatial-frequency components of the function $\varphi(S - S_c)$ are always smaller than those of the function $\varphi(S)$ when $S_c > 0$. In addition, the radial spatial frequency f_c that corresponds to the longitudinal spatial frequency S_c can be determined to be $f_c = \sqrt{2S_c/\lambda}$, according to the relation $S = \lambda f^2/2$.

Third, we use the function $\varphi(S - S_c)$ to replace the function $k\psi(\sqrt{2S/\lambda},\ 0)$ in Eq. (4) and construct an axially symmetric field distribution $\phi(r,\ z)$ by means of the integral transform

$$\phi(r,\ z) = \int_0^\infty \varphi(S - S_c)\exp(-i2\pi Sz) \times J_0(2\pi r\sqrt{2S/\lambda})\mathrm{d}S. \qquad (7)$$

The axially symmetric field $\phi(r,\ z)$ given by Eq. (7) is always a solution of the paraxial wave equation of Eq. (1). In terms of Eq. (7), the property $J_0(0) = 1$, and the Fourier transform relation

$$\sqrt{I_g(0,z)} = \int_{-\infty}^\infty \varphi(S_1)\exp(-i2\pi S_1 z)\mathrm{d}S_1,$$

one can prove that the on-axis field distribution $\phi(0,z)$ can be expressed as

$$\phi(0,z) = \exp(-i2\pi S_c z)[\sqrt{I_g(0,z)} - g(z)], \qquad (8)$$

$$g(z) = \int_{-\infty}^{-S_c} \varphi(S_1)\exp(-i2\pi S_1 z)\mathrm{d}S_1, \qquad (9)$$

where $S_1 = S - S_c$. In terms of Eq. (8), the on-axis intensity distribution $I(0,z)$ can be determined to be

$$I(0,z) = |\sqrt{I_g(0,z)} - g(z)|^2. \qquad (10)$$

As pointed out above, in the total behavior the larger the quantity S_c, the smaller the function $g(z)$, and therefore the smaller the difference between $I(0,z)$ and $I_g(0,z)$. In particular, $g(z) \to 0$ and $I(0,z) \to I_g(0,z)$ when $S_c \to \infty$.

Finally, we increase the value of the quantity S_c until the difference between $I(0,z)$ and $I_g(0,z)$ becomes negligible. Seldom, if the inverse Fourier transform $\varphi(S)$ of the function $\sqrt{I_g(0,z)}$ has no negative spatial-frequency component (namely, $\varphi(S) = 0$ for $S < 0$), the parameter S_c can be always chosen to be 0. In this case, the constructed three-dimensional field distribution $\phi(r,\ z)$ can be given by

$$\phi(r,\ z) = \int_0^\infty \varphi(S)\exp(-i2\pi Sz)J_0(2\pi r\sqrt{2S/\lambda})\mathrm{d}S.$$

One can prove that, in this special case, the constructed on-axis intensity distribution $I(0,z)$ is exactly the on-axis desired intensity distribution $I_g(0,z)$.

From the above analysis, one can find that the parameter S_c is very important. Its value has a direct influence on the difference between the constructed on-axis intensity distribution $I(0,z)$ and the on-axis desired intensity distribution $I_g(0,z)$. The larger the value of S_c, the smaller the difference between $I(0,z)$ and $I_g(0,z)$. Therefore, when the parameter S_c is large enough, the constructed on-axis intensity distribution $I(0,z)$ approaches the on-axis desired intensity distribution $I_g(0,z)$. However, it is necessary to point out that the above conclusion is valid only when the paraxial approximation is satisfied.[28] If the investigated optical field

$\phi(r, z)$ does not satisfy the paraxial approximation, the difference between $I(0,z)$ and $I_g(0,z)$ may increase with the increase of the parameter S_c. Therefore, in practical applications, one should choose the value of the parameter S_c such that the difference between $I(0,z)$ and $I_g(0,z)$ is small and at the same time the paraxial approximation is satisfied. One can use the condition $\theta_c \ll 1$ to roughly determine whether the paraxial approximation is satisfied, where $\theta_c = \lambda f_c = \sqrt{2\lambda S_c}$ is the characterization angle corresponding to the spatial frequency S_c. Fortunately, in almost all cases, the paraxial approximation is well satisfied.

3. AXIALLY SYMMETRIC ON-AXIS FLAT-TOP BEAM

As a concrete application of the above synthesis method, let us now present a new pseudo-nondiffracting beam. In this example, the on-axis desired intensity distribution $I_g(0,z)$ is the rectangular function rect$[(z - z_c)/L]$, whose value is given by rect$[(z - z_c)/L] = 1$ for the region of $|(z - z_c)/L| \leqslant 1/2$ and rect$[(z - z_c)/L] = 0$ elsewhere. The parameters L and z_c express the flat-top length and the central position of the on-axis flat-top intensity distribution rect$[(z - z_c)/L]$, respectively. Substituting the rectangular function rect$[(z - z_c)/L]$ into Eq. (6), one can determine the function $\varphi(S)$ to be

$$\varphi(S) = L \operatorname{sinc}(L\pi S)\exp(i2\pi S z_c), \tag{11}$$

where $\operatorname{sinc}(u) = \sin(u)/u$ is the sinc function.

By employing the synthesis method developed in Section 2, one can construct the complex optical field distribution $\phi(r, z)$ that corresponds to the on-axis desired intensity distribution rect$[(z - z_c)/L]$ and the parameter S_c (see Appendix A):

$$\phi(r, z) = \int_0^\infty L \operatorname{sinc}[L\pi(S - S_c)] \times \exp[i2\pi(Sz_c - S_c z_c - Sz)] \times J_0\left[2\pi r\left(\frac{2S}{\lambda}\right)^{1/2}\right] \mathrm{d}S. \tag{12}$$

In particular, the on-axis intensity distribution $I(0,z)$ can be expressed as (see Appendix B)

$$I(0,z) = |\phi(0,z)|^2 = \left|\operatorname{rect}\left(\frac{z - z_c}{L}\right) - g(z)\right|^2, \tag{13}$$

$$g(z) = \int_{-\infty}^{-S_c} L \operatorname{sinc}(L\pi S_1) \times \exp[-i2\pi S_1(z - z_c)]\mathrm{d}S_1, \tag{14}$$

where $S_1 = S - S_c$.

As we pointed out in Section 2, the larger the parameter S_c, the smaller the value of the function $g(z)$ and the smaller the difference between the on-axis intensity distribution $I(0,z)$ and the ideal flat-top profile rect$[(z - z_c)/L]$. When $S_c \to \infty$, $g(z)$ approaches 0 and the on-axis intensity distribution $I(0,z)$ approaches the ideal flat-top profile rect$[(z - z_c)/L]$. For this reason, we name the beam whose field distribution $\phi(r, z)$ is given by Eq. (12) the axially symmetric on-axis flat-top beam (AFTB). From Eq. (12) one can find that the complex optical field distribution $\phi(r, z)$ of the AFTB is completely determined by three parameters L, S_c, and z_c. As an important consequence, the on-axis intensity distribution $I(0,z)$ is also determined by the parameters L, S_c, and z_c. In fact, as we show below, the normalized on-axis intensity distribution of the AFTB is simply determined by the quantity LS_c. According to the original distribution $L \operatorname{sinc}[L\pi(S - S_c)]\exp[i2\pi(S - S_c)z_c]$ of the AFTB at the original $z = 0$ plane, the physical meaning of the parameter S_c in this example can be reasonably explained as the central spatial frequency of the AFTB. In addition, it is worth mentioning that the central position z_c can be zero or negative, according to Eq. (12). The negative z_c means only that the central position is located at the left-hand side of the $z = 0$ plane. However, we are more interested in those AFTB's with positive z_c.

To understand more clearly the influence of the parameters L, S_c, and z_c on the difference between the on-axis intensity distribution $I(0,z)$ and the ideal flat-top profile rect$[(z - z_c)/L]$, let us now introduce two dimensionless normalization parameters $\xi = LS_1$ and $\eta = (z - z_c)/L$. In terms of ξ and η, the on-axis intensity distribution $I(0, \eta)$ and the difference function $g(\eta)$ can be respectively reexpressed as (see Appendix B) $I(0, \eta) = |\operatorname{rect}(\eta) - g(\eta)|^2$ and

$$g(\eta) = \int_{-\infty}^{-LS_c} \operatorname{sinc}(\pi\xi)\exp(-i2\pi\xi\eta)\mathrm{d}\xi. \tag{15}$$

Equation (15) and the relation $I(0, \eta) = |\operatorname{rect}(\eta) - g(\eta)|^2$ explicitly show that the difference between the on-axis intensity distribution $I(0, \eta)$ and the ideal flat-top profile rect(η) is determined only by the quantity LS_c and that the larger the quantity LS_c, the smaller the difference between $I(0, \eta)$ and rect(η). One may be surprised at the property that the parameter z_c has no influence on the difference between $I(0, \eta)$ and rect(η). In our opinion, this property can be explained as follows: (1) the parameter z_c is related only to the phase factor $\exp(i2\pi Sz_c)$ in Eq. (12) [note that the constant phase factor $\exp(-i2\pi S_c z_c)$ can be ignored]; (2) according to the parallel shift theorem of Fourier transform theory, the phase factor $\exp(i2\pi Sz_c)$ creates only a parallel shift z_c in the on-axis field distribution; and (3) therefore the parameter z_c has no influence on the on-axis normalized intensity distribution $I(0, \eta)$.

The normalized on-axis intensity distributions $I(0, \eta)$ of the AFTB's for $LS_c = 10$, $LS_c = 100$, and $LS_c = 200$ are shown in Fig. 1. From Fig. 1 one can find that, just as we expected, the larger the quantity LS_c, the smaller the difference between $I(0, \eta)$ and rect(η). In the simulation of Fig. 1, we do not use Eq. (15) and the formula $I(0, \eta) = |\operatorname{rect}(\eta) - g(\eta)|^2$, but rather we directly use the equivalent formula

$$I(0, \eta) = \left|\int_{-LS_c}^{H} \operatorname{sinc}(\pi\xi)\exp(-i2\pi\xi\eta)\mathrm{d}\xi\right|^2. \tag{16}$$

In Eq. (16) the parameter H, which is used as the upper limit of the integral (to replace the real integral limit ∞) in the numerical simulation, can be chosen to be any large

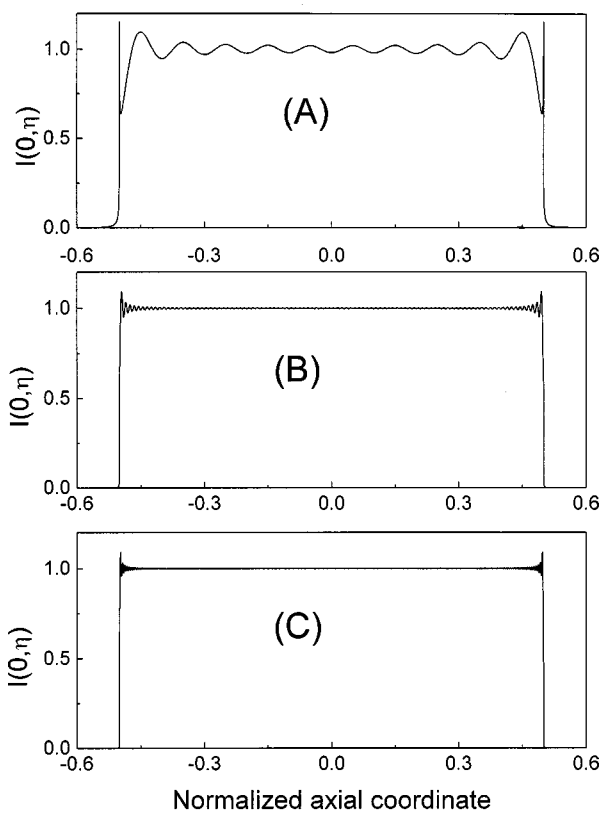

Fig. 1. Normalized on-axis intensity distributions $I(0, \eta)$ of the AFTB's for (a) $LS_c = 10$, (b) $LS_c = 100$, and (c) $LS_c = 200$.

number, such as 3000, 4000, or 5000. In the simulation of Fig. 1, we let the integral limit H be 4000. From the point of view of physics, this treatment does not lead to any difference in the physical results because the function $\mathrm{sinc}(\pi\xi)$ is actually equal to zero when $\xi > 4000$. One may be surprised at the steep edges of the on-axis normalized intensity distributions $I(0, \eta)$. In our opinion, these steep edges result from the infinite aperture effect (note that the integral limit 4000 used in the simulation is actually equivalent to the integral limit ∞ and therefore can be regarded as an infinite aperture). To make this statement clearer, we investigate the influence on the normalized on-axis intensity distribution $I(0, \eta)$ from different choices of the integral limit H. The normalized on-axis intensity distributions that correspond to different integral limits $H = 20$, $H = 50$, and $H = 100$ are shown in Figs. 2(a), 2(b), and 2(c), respectively. In Fig. 2 the value of LS_c is 10. From Fig. 2 one can see that the steep edges vanish when the parameter H is not too large. In our opinion, this is due to the finite aperture effect. By the way, Fig. 2 also shows the interesting phenomenon that, in the flat-top region, the number of large oscillations is exactly equal to LS_c and the number of small oscillations is equal to H. We emphasize that this phenomenon is not a coincidence because our numerous simulations all give the same conclusion. Perhaps it is worth further investigations in both mathematics and physics.

To support more strongly the conclusion that the parameter z_c has no influence on the on-axis normalized intensity distribution, we also directly employ Eq. (12) to present some numerical simulations (Fig. 3), which correspond to $z_c = 0.0\,\mathrm{m}$, $z_c = 5.0\,\mathrm{m}$, and $z_c = 10.0\,\mathrm{m}$, respectively. In Fig. 3 the parameters are chosen such that $L = 10\,\mathrm{m}$, $S_c = 10\,\mathrm{m}^{-1}$, $LS_c = 100$. Similarly to the treatment in Fig. 1, we also use a large number to replace the upper limit ∞ of the integral. To be consistent with the choice in Fig. 1, we let the upper limit of the integral be $410\,\mathrm{m}^{-1}$ [note that the integral region $(0\,\mathrm{m}^{-1}, 410\,\mathrm{m}^{-1})$ of the variable S in Eq. (12) is exactly equivalent to the integral region $(-100, 4000)$ of the variable ξ in Eq. (16), because of the relations $\xi = LS_1 = L(S - S_c)$, $L = 10\,\mathrm{m}$, and $S_c = 10\,\mathrm{m}^{-1}$]. Figure 3 explicitly shows that the parameter z_c has no influence on the on-axis normalized intensity distribution. In fact, Fig. 3 is completely consistent with Fig. 1(b).

From Figs. 1 and 3 one can find that there are many oscillations in the on-axis intensity distribution. It has been proven that the amplitude apodization method can efficiently suppress this kind of oscillations.[6,7,20] We are preparing to study in a future investigation how to suppress the on-axis intensity oscillations of the AFTB field by use of amplitude apodization.

It can be proved that the total energy P of the AFTB is $P = 2\pi\int_0^\infty |\psi(f, 0)|^2 f\,\mathrm{d}f$. In terms of the relation $|\psi(f, 0)| = |k^{-1}L\,\mathrm{sinc}[L\pi(S - S_c)]|$, the total energy P can be reexpressed as $P = k^{-1}L^2\int_0^\infty \mathrm{sinc}^2[L\pi(S - S_c)]\mathrm{d}S$. From this expression, one can find that the total energy P of the AFTB is always finite provided that the parameter L is finite. Fortunately, for practical ap-

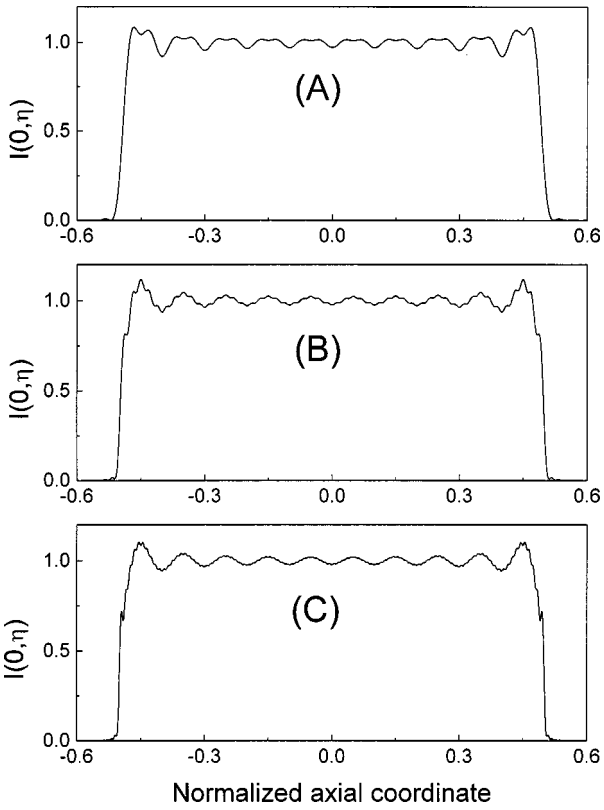

Fig. 2. Normalized on-axis intensity distribution $I(0, \eta)$ of the AFTB corresponding to $LS_c = 10$ in different choices of the high limit of the integral. (a) $H = 20$, (b) $H = 50$, and (c) $H = 100$.

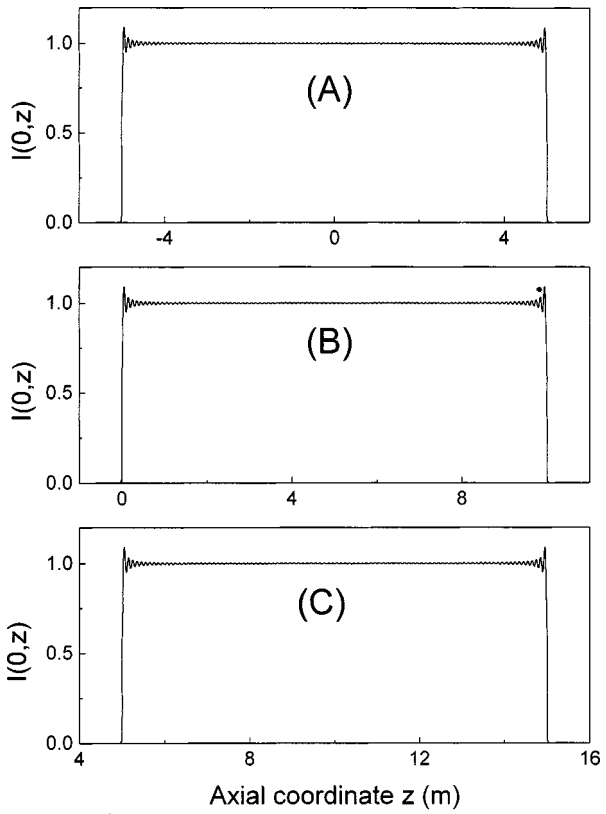

Fig. 3. On-axis intensity distribution $I(0, z)$ with different central position z_c. (a) $z_c = 0.0$ m, (b) $z_c = 5.0$ m, and (c) $z_c = 10.0$ m. The parameters L and S_c are chosen such that $L = 10$ m and $S_c = 10\ \mathrm{m}^{-1}$.

plications, the parameter L is always finite. Therefore the AFTB can be realized physically. It is apparent that the AFTB must have a beamlike shape in the transverse dimensions because its energy is finite. Figure 4 provides six transverse intensity distributions $I(r)$ of the AFTB that correspond to the $z = 0.0$-m, the $z = 9.0$-m, the $z = 9.5$-m, the $z = 9.9$-m, the $z = 10.0$-m, and the $z = 10.1$-m planes, respectively. In Fig. 4 the parameters are chosen such that $\lambda = 0.6328\ \mu$m, $L = 20$ m, $z_c = 0$ m, $S_c = 10\ \mathrm{m}^{-1}$, and $LS_c = 200$; the upper limit of the integral [Eq. (12)] is chosen to be $210\ \mathrm{m}^{-1}$ [corresponding to $H = 4000$ in Eq. (16)]. As we expected, Fig. 4 explicitly shows the transverse beamlike shape of the AFTB. In particular, Fig. 4 shows that the change of the central lobe of the transverse intensity distribution with the axial coordinate z is very small in the flat-top region. From Fig. 4 one can find that the central part of the transverse intensity distribution of the AFTB is very similar to that of the ideal Bessel J_0 beam.[1,2] This property implies that the AFTB is somewhat related to the ideal Bessel J_0 beam. In fact, as we show below, the paraxial Bessel J_0 beam is the special AFTB that corresponds to $L = \infty$. However, it is necessary to point out that, for large r, the transverse intensity distribution of the AFTB must decay faster than that of the Bessel J_0 beam, because the energy of the AFTB is always finite but the energy of the Bessel J_0 beam is infinite.

In addition, from Eq. (12) one can derive that

$$\phi(r, z)\exp(i2\pi S_c z_c) = \int_0^\infty L\,\mathrm{sinc}[L\pi(S - S_c)] \times \exp[i2\pi S(z - z_c)] \times J_0\left[2\pi r\left(\frac{2S}{\lambda}\right)^{1/2}\right]\mathrm{d}S. \quad (17)$$

Then, in terms of Eq. (17), one can further obtain

$$I(r, z_c) = |\phi(r, z_c)|^2 = \left|\int_0^\infty L\,\mathrm{sinc}[L\pi(S - S_c)]J_0\left[2\pi r\left(\frac{2S}{\lambda}\right)^{1/2}\right]\mathrm{d}S\right|^2. \quad (18)$$

Equation (18) explicitly shows that the radial intensity distribution $I(r, z_c)$ at the z_c plane is also independent of the parameter z_c. Of course, this property also results from the fact that the parameter z_c is related only to the phase factor $\exp(i2\pi S z_c)$ in the spatial-frequency distribution $\varphi(S - S_c)$.

To understand the simulations of the AFTB field better, we now briefly compare the spatial-frequency (angular spectrum) expression and the Fresnel diffraction expression. It is well known that both the (paraxial) spatial-frequency expression[28] and the Fresnel diffraction expression are the solutions of the paraxial wave equation [Eq. (1)]. They are actually equivalent, but they have different advantages. The paraxial spatial-frequency expression is more suitable for describing the near field and the quasi near field because $\psi(f, z)$ directly reduces to $\psi(f, 0)$ when $z \to 0$ [see Eq. (2)]. The Fresnel diffraction expression is more suitable for describing the far field and the quasi far field (for example, in the focal region). It is not convenient to use the Fresnel diffraction formula to evaluate the near-field and the quasi-near-field distributions (note that the flat-top region of the AFTB is of the near-field and quasi-near-field type), because this formula has a z^{-1} factor. In particular, in numerical evaluation this z^{-1} factor easily leads to large errors in those transverse planes that are close to the original $z = 0$ plane. Therefore we do not use the Fresnel diffraction formula but directly use Eq. (12) to numerically simulate the field distribution of the AFTB in this paper.

To understand the properties of the AFTB more clearly, let us now investigate the relation between the AFTB and the ideal zero-order Bessel J_0 beam.[1,2] From Eq. (12), the relation $\lim_{\pi L\to\infty} L\,\mathrm{sinc}[L\pi(S - S_c)] = \delta(S - S_c)$, and the integral property $\int_{u_0-\epsilon}^{u_0+\epsilon}\delta(u - u_0)h(u)du = h(u_0)$, one can easily obtain $\lim_{L\to\infty}\phi(r, z) = J_0(2\pi f_c r)\exp(-i\pi\lambda f_c{}^2 z)$, where $\phi(r, z)$ is given by Eq. (12), $\delta(u)$ is the Dirac δ function, ϵ is a very small quantity, and $f_c = \sqrt{2S_c/\lambda}$. On the other hand, if one use $2\pi f_c$ to replace the parameter α in Eq. (4) of Ref. 1 and then use the paraxial approximation $\beta = \sqrt{k^2 - \alpha^2} = k - \alpha^2/(2k)$, one can reexpress Eq. (4) of Ref. 1 as $E(x, y, z, t) = \exp[i(kz - \omega t)]J_0(2\pi f_c r)\exp(-i\pi\lambda f_c{}^2 z)$. Comparing these two results, one can immediately deduce that the AFTB approaches the paraxial Bessel J_0 beam[1,2] when $L \to \infty$. Therefore the AFTB can be regarded as a modified version of the paraxial Bessel J_0

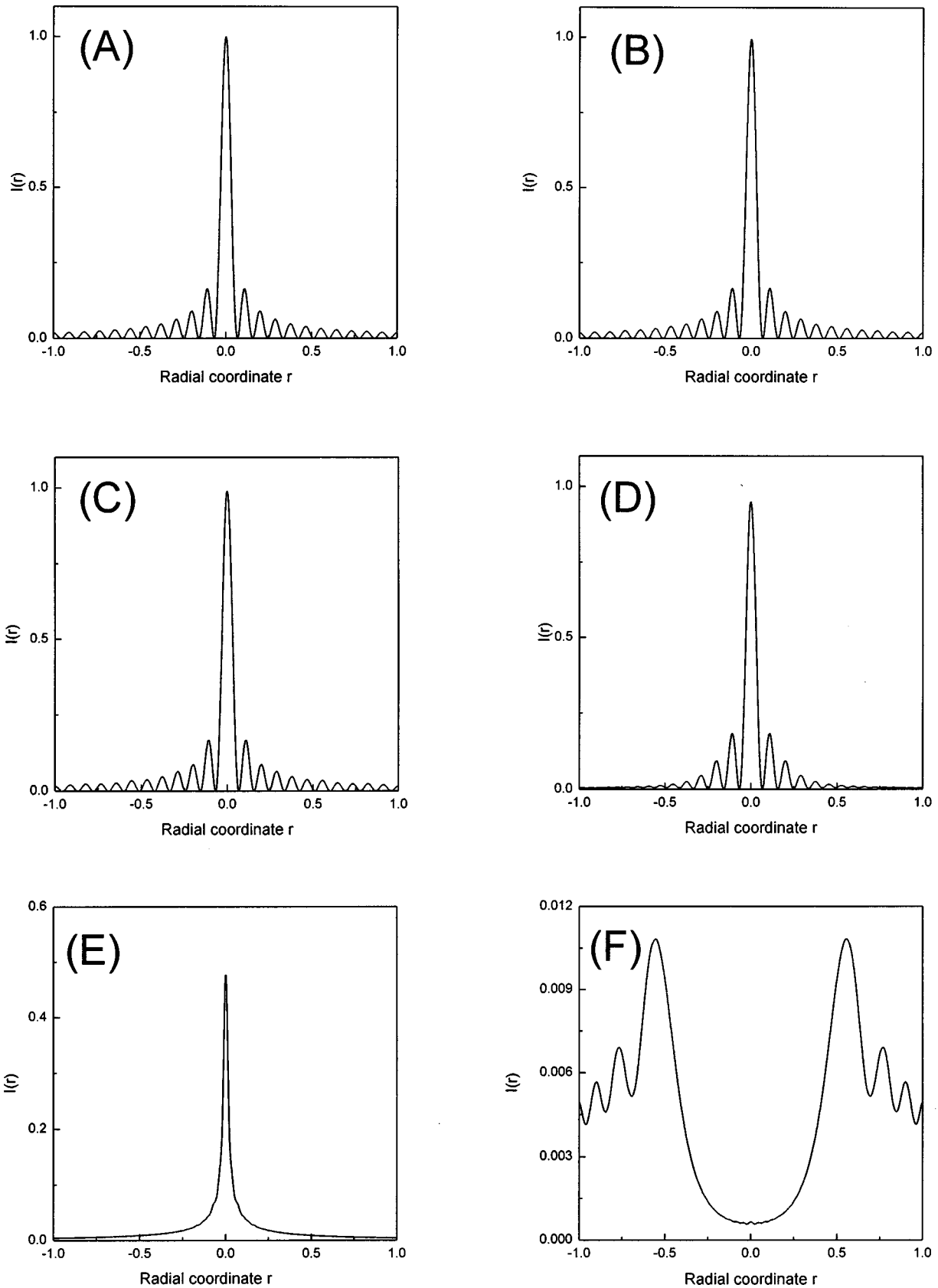

Fig. 4. Radial intensity distributions $I(r)$ of the AFTB at the (a) $z = 0.0$-m, (b) $z = 9.0$-m, (c) $z = 9.5$-m, (d) $z = 9.9$-m, (e) $z = 10.0$-m, and (f) $z = 10.1$-m planes. The parameters are chosen such that $\lambda = 0.6328\ \mu$m, $L = 20$ m, $z_c = 0$ m, $S_c = 10\ \text{m}^{-1}$, and $LS_c = 200$.

beam. This relation is helpful for understanding both the AFTB and the nondiffracting zero-order Bessel J_0 beam. Of course, it is necessary to point out that the Bessel J_0 beam generally obeys the scalar Helmholtz wave equation, but the AFTB obeys only the paraxial wave equation [Eq. (1)].

Similarly to other pseudo-nondiffracting beams, the AFTB can be generated by various methods. To be more consistent with the angular spectrum expression of Eq. (12), we suggest the following method to generate the AFTB, which is similar to the method used by Durnin *et al.*[2] We first generate the radial field distribution that is proportional to

$$L\,\mathrm{sinc}\left[L\pi\left(\frac{r_1^2}{2\lambda F^2}-S_c\right)\right]\exp\left[i2\pi z_c\left(\frac{r_1^2}{2\lambda F^2}-S_c\right)\right]\times\exp\left(-ik\frac{r_1^2}{2F}\right)$$

in the fore focal plane [the spatial frequency S in Eq. (A3) has been replaced by $r_1^2/(2\lambda F^2)$ because the relations $S=\lambda f^2/2$ and $f=r_1/(\lambda F)$], where r_1 is the radial coordinate in the fore focal plane, F is the focal length of the lens, and the phase factor $\exp[-ikr_1^2/(2F)]$ can offset the phase factor $\exp[ikr_1^2/(2F)]$ that appears in the Fraunhofer diffraction formula for the far field in focal plane. Then, according to Fourier optics theory, after the propagation through free space and the lens F, the desired AFTB field can be generated in the right-hand region of the lens F. In this generation method the property that the field distribution at the fore focal plane is proportional to the spatial-frequency distribution has been employed. This method is not suitable for generating those AFTB's that correspond to $z_c + L/2 \leqslant 0$, because, in this case, the on-axis flat-top regions of the AFTB solutions are located at the left-hand side of the lens F (i.e., the flat-top regions are not real but imaginary). Fortunately, this method is valid for those more attractive AFTB's with nonnegative z_c.

As an extension of the study of the AFTB, let us now investigate the on-axis intensity behavior of the linear superposition of multiple AFTB fields and derive the appropriate conditions for the synthesis of multiple on-axis flat-top intensity distributions. According to the linear superposition principle of optical fields, the superposition field distribution $\phi(r, z)$ of m AFTB's can be expressed as

$$\phi(r,z)=\sum_{n=1}^{m}c_n\phi_n(r,z), \tag{19}$$

$$\phi_n(r,z)=\int_0^{\infty}L_n\,\mathrm{sinc}[L_n\pi(S-S_{c,n})]\times\exp[i2\pi(Sz_{c,n}-S_{c,n}z_{c,n}-Sz)]\times J_0(2\pi r\sqrt{2S/\lambda})\mathrm{d}S, \tag{20}$$

where the subscript n corresponds to the nth AFTB. In particular, one can prove that the on-axis superposition field $\phi(0,z)$ of m AFTB's can be expressed as

$$\phi(0,z)=\sum_{n=1}^{m}c_n\exp(-i2\pi S_{c,n}z)\times\left[\mathrm{rect}\left(\frac{z-z_{c,n}}{L_n}\right)-g_n(z)\right], \tag{21}$$

$$g_n(z)=\int_{-\infty}^{-S_{c,n}}L_n\,\mathrm{sinc}(L_n\pi S_1)\times\exp[-i2\pi S_1(z-z_{c,n})]\mathrm{d}S_1. \tag{22}$$

In terms of Eqs. (21) and (22), one can easily prove that the above superposition field can give m flat-top intensity distributions on the propagation axis when the conditions $L_nS_{c,n}\gg 1$ and $2(z_{c,n+1}-z_{c,n})>L_{n+1}+L_n$ are satisfied. The conditions $2(z_{c,n+1}-z_{c,n})>L_{n+1}+L_n$ can ensure that those AFTB fields are separated by dark regions and do not interfere one another on the propagation axis. Figure 5 presents the on-axis intensity distribution of the simplest superposition field of two AFTB's. In this example the parameters are chosen such that $c_1=c_2=1$, $\lambda=0.6328\,\mu$m, $L_1=L_2=10$ m, $z_{c,1}=10$ m, $z_{c,2}=25$ m, $S_{c,1}=S_{c,2}=10\ \mathrm{m}^{-1}$, and $L_1S_{c,1}=L_2S_{c,2}=100$. Similarly to the simulation of Fig. 3, the high limit of the integral used for Fig. 5 is chosen to be $410\ \mathrm{m}^{-1}$. From Fig. 5 one can find that, just as we expected, the superposition field of the above two AFTB's indeed give two nearly flat-top intensity distributions on the propagation axis.

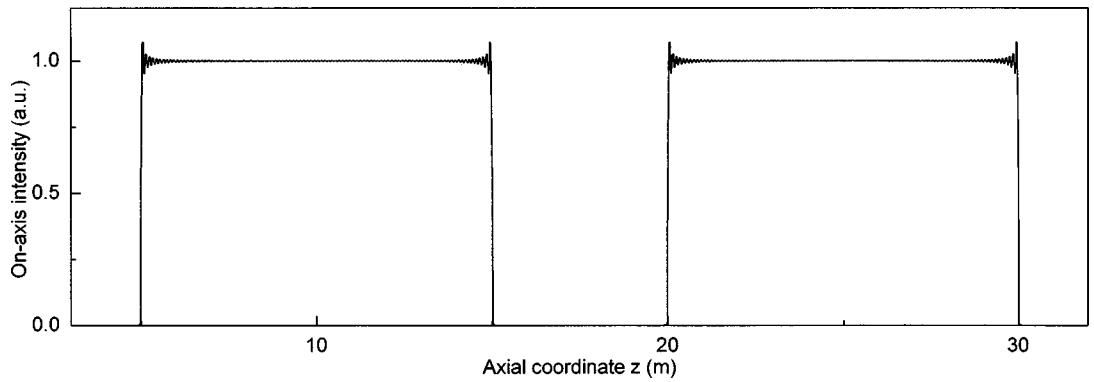

Fig. 5. On-axis intensity distribution $I(0,z)$ of the superposition field of two AFTB's. The parameters are chosen such that $c_1=c_2=1$, $\lambda=0.6328\,\mu$m, $L_1=L_2=10$ m, $z_{c,1}=10$ m, $z_{c,2}=25$ m, $S_{c,1}=S_{c,2}=10\ \mathrm{m}^{-1}$, and $L_1S_{c,1}=L_2S_{c,2}=100$.

4. CONCLUSIONS

We have employed the spatial-frequency method to construct arbitrary on-axis intensity distributions from axially symmetric fields. This synthesis method is generally valid, provided that the paraxial approximation is satisfied. As a concrete application, we have presented a new pseudo-nondiffracting beam, the axially symmetric on-axis flat-top beam (AFTB), investigated its on-axis intensity behavior, and proved that it is a modified model of the paraxial Bessel J_0 beam. In particular, we have demonstrated that the AFTB can present a nearly flat-top intensity distribution on the propagation axis when $LS_c \gg 1$. As an extension of the study of the AFTB, we have theoretically proved that the linear superposition of multiple AFTB fields can provide multiple flat-top intensity distributions on the propagation axis when the conditions $L_n S_{c,n} \gg 1$ and $2(z_{c,n+1} - z_{c,n}) > L_{n+1} + L_n$ are satisfied. In addition, we have suggested a generation method for a single AFTB field. The realization method for the superposition fields of multiple AFTB's is now under investigation.

APPENDIX A: DERIVATION OF EQ. (12)

Substituting the rectangular function $\mathrm{rect}[(z - z_c)/L]$ into Eq. (6), one can obtain

$$\varphi(S) = \int_{z_c - L/2}^{z_c + L/2} \exp(i2\pi Sz)\mathrm{d}z. \tag{A1}$$

Integrating the right-hand side of Eq. (A1), one can further obtain

$$\varphi(S) = \frac{\sin(\pi SL)}{\pi S}\exp(i2\pi Sz_c). \tag{A2}$$

which is just Eq. (11) of Section 3.

From Eq. (11), one can determine the function $\varphi(S - S_c)$ to be

$$\varphi(S - S_c) = L\,\mathrm{sinc}[L\pi(S - S_c)]\exp[i2\pi z_c(S - S_c)]. \tag{A3}$$

Then substituting Eq. (A3) into Eq. (7), one can easily derive Eq. (12) of Section 3.

APPENDIX B: DERIVATION OF EQ. (15)

From Eq. (12) and the relation $J_0(0) = 1$, one can express the on-axis field distribution $\phi(0,z)$ as

$$\begin{aligned}\phi(0,z) &= \int_0^\infty L\,\mathrm{sinc}[L\pi(S - S_c)] \\ &\quad \times \exp[i2\pi(Sz_c - S_c z_c - Sz)]\mathrm{d}S \\ &= \exp(-i2\pi S_c z)\int_0^\infty L\,\mathrm{sinc}[L\pi(S - S_c)] \\ &\quad \times \exp[-i2\pi(S - S_c)(z - z_c)]\mathrm{d}S. \end{aligned}\tag{B1}$$

Then, in terms of the variable $S_1 = S - S_c$, the field $\phi(0,z)$ can be further expressed as

$$\begin{aligned}\phi(0,z) &= \exp(-i2\pi S_c z)\int_{-S_c}^\infty L\,\mathrm{sinc}(L\pi S_1) \\ &\quad \times \exp[-i2\pi S_1(z - z_c)]\mathrm{d}S_1. \end{aligned}\tag{B2}$$

Note that the integral low limit has been varied to $-S_c$ from 0.

By employing the Fourier transform relation

$$\begin{aligned}\mathrm{rect}\left(\frac{z - z_c}{L}\right) &= \int_{-\infty}^\infty L\,\mathrm{sinc}(L\pi S_1)\exp(i2\pi S_1 z_c) \\ &\quad \times \exp(-i2\pi S_1 z)\mathrm{d}S_1, \end{aligned}$$

one can reexpress Eq. (B2) as

$$\phi(0,z)\exp(i2\pi S_c z) = \mathrm{rect}\left(\frac{z - z_c}{L}\right) - g(z), \tag{B3}$$

$$\begin{aligned} g(z) &= \int_{-\infty}^{-S_c} L\,\mathrm{sinc}(L\pi S_1) \\ &\quad \times \exp[-i2\pi S_1(z - z_c)]\mathrm{d}S_1, \end{aligned}\tag{B4}$$

where the relation $\int_{-S_c}^{\infty} = \int_{-\infty}^{\infty} - \int_{-\infty}^{-S_c}$ has been used. Obviously, Eqs. (13) and (14) are the direct consequence of Eqs. (B3) and (B4).

It is apparent that $g(z)$ can be reexpressed as

$$\begin{aligned} g(z) &= \int_{-\infty}^{-LS_c} \mathrm{sinc}[\pi(LS_1)] \\ &\quad \times \exp\left[-i2\pi(LS_1)\frac{z - z_c}{L}\right]\mathrm{d}(LS_1). \end{aligned}\tag{B5}$$

If we use the dimensionless normalized parameters $\xi = LS_1$ and $\eta = (z - z_c)/L$, then Eq. (B5) can be further expressed as

$$g(\eta) = \int_{-\infty}^{-LS_c} \mathrm{sinc}(\pi\xi)\exp(-i2\pi\xi\eta)\mathrm{d}\xi, \tag{B6}$$

where we have used $g(\eta)$ to replace $g(z)$ because the right-hand side of Eq. (B6) is a single-variable function of the dimensionless parameter η.

Substituting Eq. (B6) into Eq. (B3), one can derive

$$I(0,\eta) = |\mathrm{rect}(\eta) - g(\eta)|^2, \tag{B7}$$

where $g(\eta)$ is given by Eq. (B6). Note that Eq. (B6) is just Eq. (15) of Section 3. As an important consequence of Eqs. (B7) and (B6), the normalized on-axis intensity distribution $I(0,\eta)$ is related only to the quanty LS_c.

ACKNOWLEDGMENTS

This research was partially supported by the National Science Council of China under contract NSC 88-2215-E-009-006. The authors are indebted to Lee W. Casperson and the reviewers for their comments and proposals for improving the paper.

*Also with Shanghai Institute of Optics and Fine Mechanics, Chinese Academy of Sciences, P.O. Box 800-211, Shanghai 201800, China.

REFERENCES

1. J. Durnin, "Exact solutions for nondiffracting beams. I. The scalar theory," J. Opt. Soc. Am. A **4**, 651–654 (1987).
2. J. Durnin, J. J. Miceli, Jr., and J. H. Eberly, "Diffraction-free beams," Phys. Rev. Lett. **58**, 1499–1501 (1987).
3. J. Turunen, A. Vasara, and A. T. Friberg, "Holographic generation of diffraction-free beams," Appl. Opt. **27**, 3959–3962 (1988).
4. A. Vasara, J. Turunen, and A. T. Friberg, "Realization of general nondiffracting beams with computer-generated holograms," J. Opt. Soc. Am. A **6**, 1748–1754 (1989).
5. A. J. Cox and D. C. Dibble, "Holographic reproduction of a diffraction-free beam," Appl. Opt. **30**, 1330–1332 (1991).
6. A. J. Cox and J. D'Anna, "Constant-axial-intensity nondiffracting beam," Opt. Lett. **17**, 232–234 (1992).
7. Z. Jaroszewich, J. Sochacki, A. Kolodziejczyk, and L. R. Staronski, "Apodized annular-aperture logarithmic axicon: smoothness and uniformity of intensity distributions," Opt. Lett. **18**, 1893–1895 (1993).
8. R. Piestun and J. Shamir, "Control of wave-front propagation with diffractive elements," Opt. Lett. **19**, 771–773 (1994).
9. B. Salik, J. Rosen, and A. Yariv, "One-dimensional beam shaping," J. Opt. Soc. Am. A **12**, 1702–1706 (1995).
10. J. Rosen, B. Salik, A. Yariv, and H. K. Liu, "Pseudonondiffracting slitlike beam and its analogy to the pseudonondispersing pulse," Opt. Lett. **20**, 423–425 (1995).
11. J. Rosen, B. Salik, and A. Yariv, "Pseudo-nondiffracting beams generated by radial harmonic functions," J. Opt. Soc. Am. A **12**, 2446–2457 (1995).
12. Z. Jiang, Q. Lu, and Z. Liu, "Propagation of apertured Bessel beams," Appl. Opt. **34**, 7183–7185 (1995).
13. B.-Z. Dong, G.-Z. Yang, B.-Y. Gu, and O. K. Ersoy, "Iterative optimization approach for designing an axicon with long focal depth and high transverse resolution," J. Opt. Soc. Am. A **13**, 97–103 (1996).
14. A. T. Friberg, "Stationary-phase analysis of generalized axicons," J. Opt. Soc. Am. A **13**, 743–750 (1996).
15. L. Niggl, T. Lanzl, and M. Maier, "Properties of Bessel beams generated by periodic grating of circular symmetry," J. Opt. Soc. Am. A **14**, 27–33 (1997).
16. S. Y. Popov and A. T. Friberg, "Design of diffractive axicons for partially coherent light," Opt. Lett. **23**, 1639–1641 (1998).
17. W.-X. Cong, N.-X. Chen, and B.-Y. Gu, "Generation of nondiffracting beams by diffractive phase elements," J. Opt. Soc. Am. A **15**, 2362–2364 (1998).
18. M. Honkanen and J. Turunen, "Tandem systems for efficient generation of uniform-axial-intensity Bessel fields," Opt. Commun. **154**, 368–375 (1998).
19. S. Y. Popov and A. T. Friberg, "Apodization of generalized axicons to produce uniform axial line images," Pure Appl. Opt. **7**, 537–548 (1998).
20. A. G. Sedukhin, "Beam-preshaping axicon focusing," J. Opt. Soc. Am. A **15**, 3057–3066 (1998).
21. Z. Jaroszewicz and J. Morales, "Lens axicons: systems composed of a diverging aberrated lens and a perfect converging lens," J. Opt. Soc. Am. A **15**, 2383–2390 (1998).
22. Z. Jaroszewicz and J. Morales, "Lens axicons: systems composed of a diverging aberrated lens and a converging aberrated lens," J. Opt. Soc. Am. A **16**, 191–197 (1999).
23. N. Guérineau and J. Primot, "Nondiffracting array generation using an N-wave interferometer," J. Opt. Soc. Am. A **16**, 293–298 (1999).
24. J. Rosen and A. Yariv, "Synthesis of an arbitrary axial field profile by computer-generated holograms," Opt. Lett. **19**, 843–845 (1994).
25. R. Piestun, B. Spektor, and J. Shamir, "Wave fields in three dimensions: analysis and synthesis," J. Opt. Soc. Am. A **13**, 1837–1848 (1996).
26. R. Liu, B.-Z. Dong, G.-Z. Yang, and B.-Y. Gu, "Generation of pseudo-nondiffracting beams with use of diffractive phase elements designed by the conjugate-gradient method," J. Opt. Soc. Am. A **15**, 144–151 (1998).
27. R. Liu, B.-Y. Gu, B.-Z. Dong, and G.-Z. Yang, "Design of diffractive phase elements that realize axial-intensity modulation based on the conjugate-gradient method," J. Opt. Soc. Am. A **15**, 689–694 (1998).
28. See, for examples, J. W. Goodman, *Introduction to Fourier Optics*, 2nd ed. (McGraw-Hill, New York, 1996), pp. 55–58 and pp. 11–12; G. P. Agrawal and D. N. Pattanayak, "Gaussian beam propagation beyond the paraxial approximation," J. Opt. Soc. Am. **69**, 575–578 (1979); Q. Cao and X. Deng, "Corrections to the paraxial approximation of an arbitrary free-propagation beam," J. Opt. Soc. Am. A **15**, 1144–1148 (1998).